

# Multimode Operation of a PV-Battery System fed Brushless DC Motor Drive

N. Sai Vinay Kishore<sup>a</sup>, Naresh P<sup>b</sup>, V. Seshadri Sraavan Kumar<sup>c</sup>, *Member, IEEE*

Department of Electrical Engineering

Indian Institute of Technology (IIT) Hyderabad, INDIA

<sup>a</sup>ee18mtech11034@iith.ac.in, <sup>b</sup>ee17resch11014@iith.ac.in, <sup>c</sup>seshadri@ee.iith.ac.in

**Abstract**—Utilization of energy storage systems along with Photovoltaic systems, can provide an efficient solution to overcome the challenges associated with renewable energy sources. This paper proposes an algorithm for the multimode operation of a Brushless DC motor drive fed using a combination of Photovoltaic System and battery-based energy storage. Based on the solar irradiation and the state of charge of the battery, the proposed algorithm identifies a control scheme wherein the entire system operates in Four different modes. The working of the PV-Battery System fed Brushless DC Motor Drive under various operating modes is presented and is verified using simulation analysis performed in MATLAB/Simulink.

**Index Terms**—Brushless DC motor, multimode operation, maximum power point tracking, lower power point tracking, state of charge

## I. INTRODUCTION

Environmental concerns, the decline in fossil fuels, and the sustained enhancement in the technologies related to power electronics [1]–[3] have led to the development of power generation from renewable energy sources. Among the available renewable energy technologies, Photovoltaic (PV) systems have gained popularity due to its unique advantage of having less (or no) restrictions on its establishment location. As a result, PV based applications (both grid-connected and standalone) have gained much attention in the past decade. Similarly, Brushless DC (BLDC) motors have also been gaining popularity in recent times. As a result of its compact size, high-speed range, and high power to weight ratio [4], the BLDC motors are being preferred over other motors in few standalone applications such as electric vehicles, water pumping applications. This paper focuses on the multimode operation of a standalone PV system feeding a drive.

Several approaches have been proposed in the literature [5]–[8] for the operation of PV based BLDC drives. The design and control of a PV fed BLDC motor which feeds a water pumping system and supplies energy to a single-phase utility grid, is reported in [7]. The design and advantages of ferrite magnet type BLDC motor used in PV based pump applications are discussed in [6]. A single stage PV-BLDC configuration that avoids the use of the DC/DC converter is presented in [9]. M. R. Feyzi *et.al.* [8] propose a control strategy for operation of

This work is supported by the Department of Science and Technology (DST), Government of INDIA through the INSPIRE research grant DST/INSPIRE/04/2016/002381

a BLDC drive fed by a hybrid energy system, which includes either a PV, a fuel cell (FC) or a battery as a source.

One of the challenges associated with the utilization of PV system as a primary source is the variation in the available power due to changes in weather conditions. One way to overcome this challenge is to utilize an energy storage device along with the PV system. This paper presents an algorithm for the multimode operation of BLDC motor fed by the PV system and a battery.

This paper is organized as follows. Section II of the manuscript describes the topology and associated mathematical modeling of a PV-Battery fed BLDC drive. The control of the boost and the bidirectional DC/DC converter associated with the proposed configuration is also described in Section II. Section III presents the proposed multimode algorithm. Validation of the proposed algorithm using simulations is reported in Section IV followed by conclusions in Section V.

## II. MODELING AND CONTROL OF A PV-BATTERY SYSTEM FED BRUSHLESS DC MOTOR DRIVE

The energy source of the system comprises of a PV system (primary source) and a battery pack (secondary source). The primary source (i.e. the PV panel) is integrated to the DC link via a boost converter while the secondary source (i.e. the battery) is integrated to the DC link via a bidirectional DC/DC converter. The BLDC motor is fed from the DC link via a 3- $\phi$  inverter operating in 120° conduction mode. The schematic diagram of the complete system is shown in Fig. 1.

The primary function of the boost converter is to regulate the output power of a PV panel. On the other hand, the

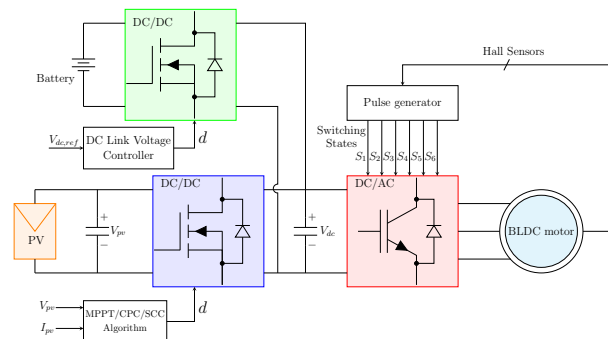


Fig. 1: Schematic diagram of a PV-Battery fed BLDC drive

bidirectional converter associated with the battery is designed to maintain a constant DC link voltage (so that the power balance is achieved). Maintaining a constant DC link voltage ensures an easier control of BLDC motor drive.

To start with, the mathematical models employed for modeling are outlined in brief (for the purpose of completeness).

#### A. Modeling of PV panel

In this paper, the PV system is modeled based on the equivalent single-diode model of a PV cell (as shown in Fig. 2). The non-idealities present in the PV panel are represented

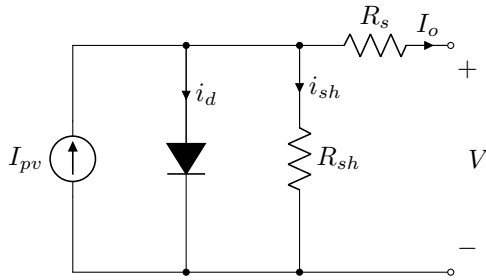


Fig. 2: Equivalent circuit of a PV cell

by an equivalent series and parallel resistances ( $R_s$  and  $R_p$  respectively). Based on the equivalent circuit of a PV cell, the output current can be written as

$$I = I_{pv} - I_o \left[ \exp\left(\frac{V + R_s I}{aV_t}\right) - 1 \right] - \frac{V + R_s I}{R_p} \quad (1)$$

where  $V$  and  $I$  represent the terminal voltage and the output current, respectively.  $I_{pv}$  and  $I_o$  represent the photovoltaic and saturation currents, respectively.  $V_t$  represents the thermal voltage, and  $a$  is the diode ideality factor.

In general, a PV array is the combination of various PV cells connected in series or parallel, to achieve the required voltage and current. If  $N_s$  and  $N_p$  are the number of PV cells connected in series and parallel respectively, then the PV array current ( $I_a$ ) and terminal voltage ( $V_a$ ) are related by (2). The detailed design of the PV panel is reported in [10].

$$I_a = N_p I_{pv} - N_p I_o \left[ \exp\left(\frac{\frac{V_a}{N_s} + I_a \frac{R_s}{N_p}}{aV_t}\right) - 1 \right] - \frac{V_a \frac{N_p}{N_s} + R_s I_a}{R_p} \quad (2)$$

#### B. Modeling of Battery

Some of the most commonly adopted models for batteries include experimental based, electrochemical based and electric circuit-based models. However, for the estimation and analysis based on state-of-charge (SoC), the electric circuit models are preferable [11] and hence have been adopted in this work. A typical circuit based representation of a battery consists of a dependent voltage source with a series resistance (i.e. internal resistance  $R_b$ ) as shown in Fig. 3. Based on the equivalent circuit model, the terminal voltage of the battery can be written as,

$$V_b = E - iR_b \quad (3)$$

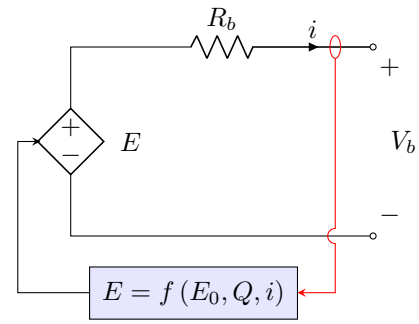


Fig. 3: Equivalent Circuit of Battery

where  $E$  is the no-load voltage and  $i$  is the terminal current. Typically, the value of  $E$  is a function of open circuit voltage ( $E_0$ ), the capacity of the battery ( $Q$  in Ah) and the terminal current ( $i$ ). The exact dependence of  $E$  (i.e.  $E = f(E_0, Q, i)$ ) was first proposed by shepherd [12]. However, in order avoid simulation issues arising out of the infinite loop this works adopts the modified shepherd model proposed in [11]. Accordingly, the no-load voltage is given by

$$E = E_o - K \frac{Q}{Q - it} + A \exp(-B.it) \quad (4)$$

For a given battery, the parameters of the model was estimated using the approach outlined in [11].

#### C. Modeling of Brushless DC motor

Under balanced operation (i.e.  $i_{as} + i_{bs} + i_{cs} = 0$ ), the dynamic equations (related to electrical port) describing the behavior of BLDC motor [13] are given by

$$\begin{aligned} v_{as} &= R_s i_{as} + (L - M) \frac{di_{as}}{dt} + e_{as} \\ v_{bs} &= R_s i_{bs} + (L - M) \frac{di_{bs}}{dt} + e_{bs} \\ v_{cs} &= R_s i_{cs} + (L - M) \frac{di_{cs}}{dt} + e_{cs} \end{aligned} \quad (5)$$

where  $R_s$  is the resistance per phase of the stator winding. The induced EMFs  $e_{as}$ ,  $e_{bs}$  and  $e_{cs}$  are assumed to be ideal (i.e. having trapezoidal wave shape as shown in Fig. 4) and can be written as

$$\begin{aligned} e_{as} &= K_b f_{as}(\theta_r) \omega_m \\ e_{bs} &= K_b f_{bs}(\theta_r) \omega_m \\ e_{cs} &= K_b f_{cs}(\theta_r) \omega_m \end{aligned} \quad (6)$$

where  $\omega_m$  is the mechanical speed of the motor and  $\theta_r$  is the rotor position (which is determined by using the Hall sensor signals  $H_a$ ,  $H_b$  and  $H_c$ ). Further, under the ideal back emf assumption,  $f_{as}(\theta_r)$  can be written as

$$f_{as}(\theta_r) = \begin{cases} \left(\frac{6}{\pi}\right) \theta_r & 0 \leq \theta_r \leq \frac{\pi}{6} \\ 1 & \frac{\pi}{6} \leq \theta_r \leq \frac{5\pi}{6} \\ \frac{6}{\pi} (\pi - \theta_r) & \frac{5\pi}{6} \leq \theta_r \leq \frac{7\pi}{6} \\ -1 & \frac{7\pi}{6} \leq \theta_r \leq \frac{11\pi}{6} \\ \frac{6}{\pi} (\theta_r - 2\pi) & \frac{11\pi}{6} \leq \theta_r \leq 2\pi \end{cases} \quad (7)$$

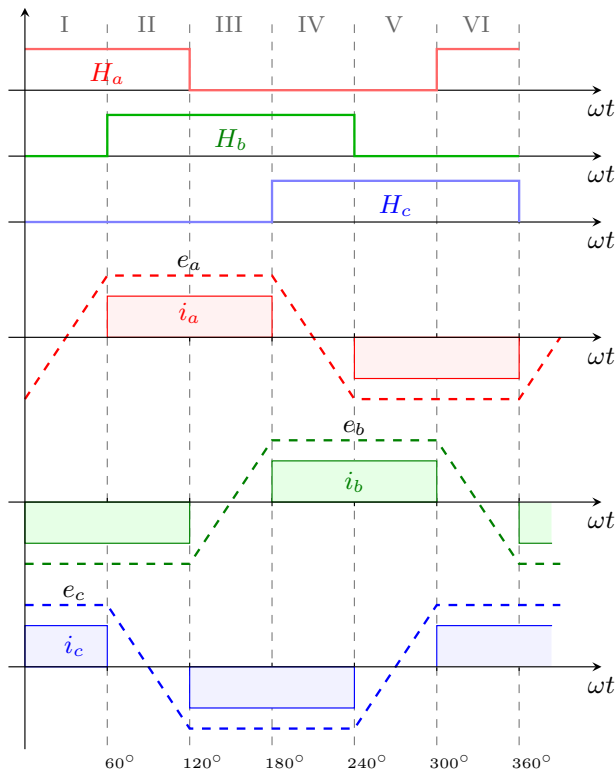


Fig. 4: Exciting sequence and corresponding Back emf of BLDC motor.

The other functions for computing the back emf of  $b$  and  $c$  phases can be computed as

$$\begin{aligned} f_{bs}(\theta_r) &= f_a(\theta_r - \frac{2\pi}{3}) \\ f_{cs}(\theta_r) &= f_a(\theta_r + \frac{2\pi}{3}) \end{aligned} \quad (8)$$

The dynamic equation related to the mechanical port is given by

$$J \frac{d\omega_m}{dt} + B\omega_m = T_{em} - T_l \quad (9)$$

where  $J$  and  $B$  represent the moment of inertia and damping coefficient of BLDC motor, respectively. The load torque is denoted by  $T_l$  and the electromagnetic torque denoted by  $T_{em}$  can be computed as

$$T_{em} = \frac{e_{as}i_{as} + e_{bs}i_{bs} + e_{cs}i_{cs}}{\omega_m} = 2K_b i_{as} \quad (10)$$

#### D. Control of the boost converter

The primary function of the boost converter (associated with the PV system) is to track a desired value of power from the PV panel. The desired value can either be the maximum value of available power (i.e. the boost converter is operating in maximum power point tracking (MPPT) mode) or a reduced value (i.e. the boost converter is operating in limited power point tracking (LPPT) mode). For a given mode of operation (determined by the multimode operational algorithm outlined in Section III), the boost converter is controlled a slightly

modified variant of the constant power tracking algorithm proposed in [14] wherein the duty ratio of the boost converter to track desired output power.

#### E. Control of the bidirectional DC/DC converter

The primary function of the bidirectional DC-DC converter (consisting of two complementary switches  $S_1$  and  $S_2$  as shown in Fig. 5) is to maintain a constant DC link voltage. In order

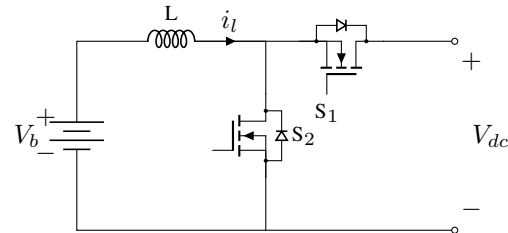


Fig. 5: Circuit diagram of a bidirectional DC/DC converter

to control the DC link voltage to a desired value, this work adopts a pulse width modulation (PWM) based dual loop control architecture (i.e. inner current control and outer voltage control) as shown in Fig. 6. The plant transfer function ( $G_i(s)$ )

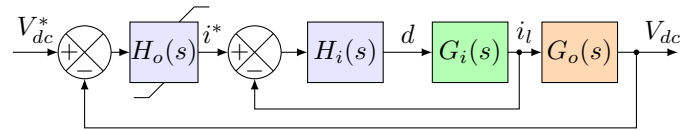


Fig. 6: Dual loop control for DC link voltage regulation

that relates the inductor current to the duty ratio) can be computed using state space averaging [15] approach as

$$G_i(s) = \frac{\hat{i}_L(s)}{\hat{d}(s)} = \frac{V_o}{R_L(1-D)^2} \frac{[sR_L C_f + 2]}{\frac{LC_f}{(1-D)^2} s^2 + \frac{L}{(1-D)^2 R_L} s + 1} \quad (11)$$

Similarly, the plant transfer function corresponding to the outer control loop ( $G_o(s)$ ) can be derived as

$$G_o(s) = \frac{\hat{V}_{dc}(s)}{\hat{i}_L(s)} = \frac{R_L(1-D) \left[ 1 - s \frac{L}{R_L(1-D)^2} \right]}{sR_L C_f + 2} \quad (12)$$

where  $R_L$  is the apparent load resistance. The frequency response corresponding to the inner and outer loop plant transfer function (corresponding to one operating point) is shown in Fig. 7. It can be observed that at higher frequencies the phase of the plant is close to  $90^\circ$  (resulting in a very good phase margin  $\phi_m$ ) and hence, a simple PI controller (given by (13)) is chosen for inner and outer loops.

$$H_i(s) = K_i \left( 1 + \frac{\omega_i}{s} \right) \text{ and } H_o(s) = K_o \left( 1 + \frac{\omega_o}{s} \right) \quad (13)$$

The gain parameters of the controller ( $K_i$  and  $K_o$ ) are selected such that the open-loop gain of the compensated system (i.e., plant and controller) is unity at the crossover frequency ( $f_{gc}$ ). Typically, the gain crossover frequencies of the current and

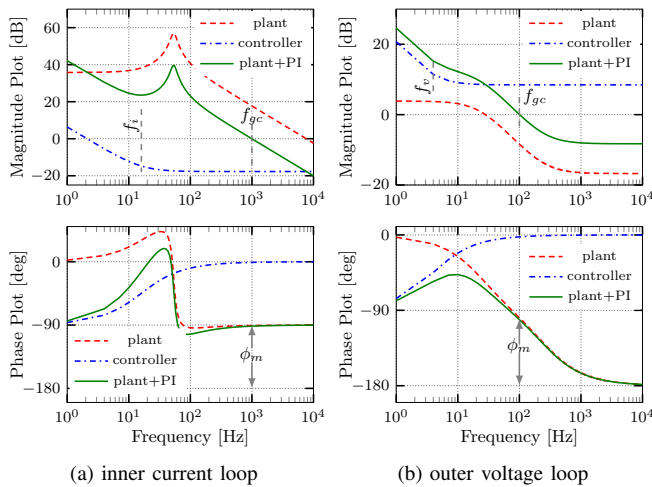


Fig. 7: Frequency response of inner and outer control loops

voltage control loops are chosen to be one-tenth and one-hundredth of the switching frequency ( $f_{sw}$ ) [16]. In this work, the switching frequency of the bidirectional converter is chosen to be 10 kHz and accordingly, the gain crossover frequencies for inner and outer-loop are 1 kHz and 0.1 kHz. The values of  $\omega_{ic}$  and  $\omega_{iv}$  are determined to make the steady-state error zero [15] (without significantly altering the gain crossover frequency), and typically these values range one-fifth to one-tenth of the gain crossover frequency [17]. The frequency response of the resulting open-loop transfer function (i.e., after the addition of controller) of inner and outer control loops is shown in Fig. 7.

### III. MULTIMODE OPERATION AND STATE TRANSITION DIAGRAM

Depending on the solar irradiation (i.e., the maximum possible output power) and the SoC of the battery, a PV-Battery fed BLDC motor drive can operate in 4 different modes, as shown in Fig. 8. The behavior and the corresponding control targets of the various sub-systems under each operating state is as follows.

- 1) State  $S_0$ : The system operates in state  $S_0$  when the output power of the PV panel is higher than the power

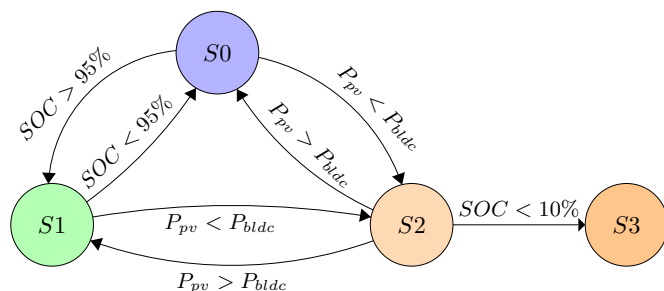


Fig. 8: State diagram for Multimode operation of PV-Battery fed BLDC drive

required for BLDC, i.e.,  $P_{pv} > P_{BLDC}$  and SoC of the battery is in between 10% to 95%. During this state, the bidirectional DC/DC converter charges the battery (i.e., stores the excess power generated by the PV panel) while the boost converter is operated in MPPT mode.

- 2) State  $S_1$ : The system operates in state  $S_1$  when the output power of the PV panel is higher than the power required for BLDC i.e.,  $P_{pv} > P_{BLDC}$  and SoC of the battery is greater than 95%. In this mode, the boost converter is operated in limited power point tracking mode (LPPT), with the reference power being the power required by the BLDC. Since the power balance is achieved by the boost converter (thereby ensuring a constant DC link voltage), the bidirectional duty ratio of the DC/DC converter will be such that the average current from the battery is 0. However, there is some current ripple in the converter currents due to the commutation ripple arising out of BLDC operation.
- 3) State  $S_2$ : The system operates in state  $S_2$  when the output power of the PV panel is lower than the power required for BLDC, i.e.,  $P_{pv} < P_{BLDC}$  and SoC of the battery is greater than 10%. In this mode, the boost converter is operated in MPPT mode, and the bidirectional DC/DC converter feeds the additional power required to drive the BLDC.
- 4) State  $S_3$ : If the available power from the PV panel is not sufficient to drive the BLDC motor and the SoC of the battery is less than 10%, the BLDC is turned off by blocking all the pulses to switches of the inverter, and the PV power is stored in the battery. During this mode, the boost converter is operated in MPPT mode.

The operating conditions (or decision variables) that determine the transition from one operating state to the other are indicated along the edges of the state transition diagram.

### IV. SIMULATION ANALYSIS

In order to indicate the performance of the proposed multimode algorithm, simulation results on the PV-Battery fed BLDC system (modeled in MATLAB/ Simulink software) are presented. The system considered for the study comprises of a 2.1Nm BLDC motor (parameters given in Table I) fed by a PV panel comprising of 2 series-connected strings (data given in Table II). On the other hand, the battery is a 48 V, 10 Ah battery. In this work, we primarily focus on evaluating the effectiveness of designed controllers during state transitions.

TABLE I: Parameters of 2.1Nm BLDC motor

BLDC parameters	
Rated Torque (Nm)	2.1
Torque Constant (Nm/A)	0.11
Back EMF (V/KRPM)	11.5
R ( $\Omega$ /phase)	0.16
L (mH/phase)	0.3
Rotor inertia ( $g \cdot cm^2$ )	2400

TABLE II: PV panel specifications

PV Panel			
Rated maximum power ( $P_{\max}$ )		345 W	
Voltage at $P_{\max}$	37.35V	Current at $P_{\max}$	9.05A
Open-Circuit voltage	46.7V	Short-Circuit current	9.58A
PV Array			
Series connected ( $N_s$ )	2	Parallel connected ( $N_p$ )	1
Rated maximum power ( $P_{\max}$ )		690 W	

Hence, the results pertaining to the PV-battery fed BLDC configuration under state transitions are reported.

- Case A: In the first case, the system is assumed to be initially operating in state  $S_0$ . At  $t = 4$  s, the solar intensity is presumed to gradually reduce (as shown in Fig. 9(a)) to less than 50% of its initial value. This drop in solar intensity causes the output power from the PV panel to reduce thereby, forcing the BLDC motor drive to draw power from the battery. Since the battery is charged close to its rated value, the system would transit from operating state  $S_0$  to state  $S_2$ . The response of the system during this transition is shown in Fig. 9. The bidirectional DC/DC converter ensures that the voltage at the DC link is controlled to a rated value of 96 V (as shown in Fig. 9(b)). Prior to  $t = 4$ s, the current through the bidirectional DC/DC converter is negative, indicating that the battery is charging. During the transition, the current gradually reverses its polarity with the battery delivering power during the new operating state. The back EMF and phase currents of the BLDC motor in state  $S_2$  is shown in Fig. 9(d). The ripple in the DC link voltage, battery current is due to the commutation ripple of the BLDC motor.

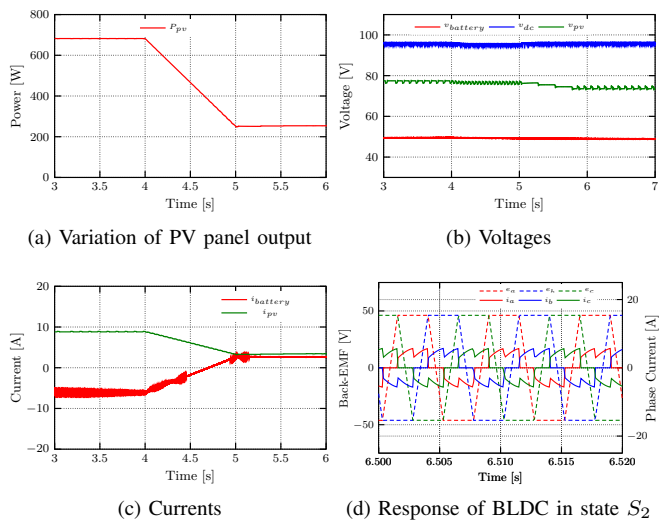


Fig. 9: Response of the PV-Battery fed BLDC drive during transition from modes  $S_0$  to  $S_2$

- Case B: The second case study aims to indicate the response of the system during the transition from state  $S_0$  to  $S_1$  (shown in Fig. 10). Accordingly, the initial operating conditions are chosen such that the PV system feeds the BLDC motor and charges the battery (i.e., the battery current is negative as shown in Fig. 10(c)). As the system continues to operate in state  $S_0$ , the SoC of the battery reaches its upper limit at around  $t = 5$  s. Hence at  $t = 5$  s, the boost converter is set to operate in LPPT mode resulting in the output power from the PV system adjusting itself to the power required by the BLDC motor (as shown in Fig. 10(a)). On the other hand, the current through the bidirectional DC/DC converter gradually reduces to zero (average value), as shown in Fig. 10(c). As indicated in Section III, there will be a small ripple in the battery current (as shown in Fig. 10(c)) due to the commutation current ripple of the BLDC motor.

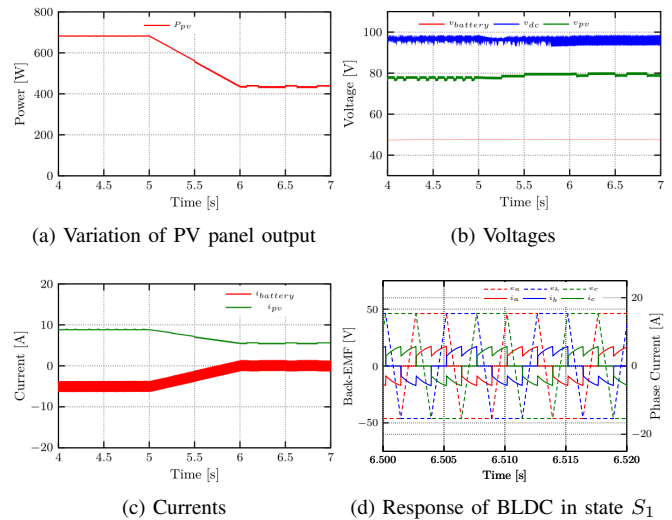


Fig. 10: Response of the PV-Battery fed BLDC drive during transition from modes  $S_0$  to  $S_1$

- Case C: In the final case study, the response of the system during transition from state  $S_1$  to  $S_2$  (shown in Fig. 11) is presented. The initial operating conditions are chosen such that the system is operating in state  $S_1$  (i.e., the average battery current is zero, as shown in Fig. 11(c)) and the PV panel is supplying the power required for BLDC). At  $t = 5$  s, it is assumed that there is a dip in solar intensity, causing the power extracted from the PV panel to fall (as shown in Fig. 11(a)). Under such a scenario, the DC link voltage controller associated with the bidirectional DC/DC converter ensures that the additional power required for BLDC is tracked from the battery (i.e., the average current from the battery is positive as shown in Fig. 11(c)).

In all the three state transitions (shown in Fig. 9-Fig. 11), it can be observed that the controllers associated with the bidirectional DC/DC converter and the boost converter are

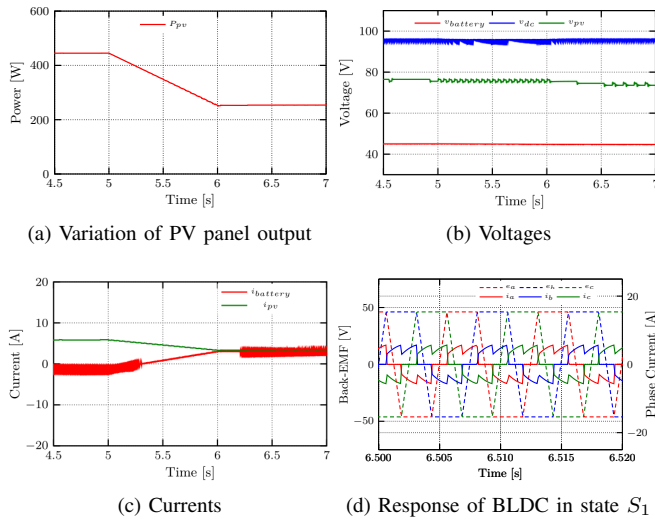


Fig. 11: Response of the PV-Battery fed BLDC drive during transition from modes  $S_1$  to  $S_2$

effective in maintaining a constant DC link voltage. On the flip side, the commutation ripple caused by the  $120^\circ$  operation of the inverters is very significant. It causes a significant ripple in the current drawn from the battery (which needs to be reduced).

## V. CONCLUSIONS

This paper proposes an algorithm for the Multimode operation of a BLDC motor drive fed by a combination of a Photovoltaic system and a battery. The proposed algorithm comprises of 4 different operating modes that are determined based on the solar irradiation and SoC of the battery. Simulation results carried out on the test system indicate the effectiveness of the proposed algorithm in handling the variations associated with the PV system. Our future work in this direction is to validate the proposed multimode algorithm experimentally and develop a switching/control scheme to reduce the ripple arising due to commutation.

## REFERENCES

- [1] B. K. Bose, "Power electronics, smart grid, and renewable energy systems," *Proceedings of the IEEE*, vol. 105, no. 11, 2017.
- [2] M. G. Molina, "Energy storage and power electronics technologies: A strong combination to empower the transformation to the smart grid," *Proceedings of the IEEE*, vol. 105, no. 11, pp. 2191–2219, 2017.
- [3] F. Blaabjerg, F. Iov, R. Teodorescu, and Z. Chen, "Power electronics in renewable energy systems," in *2006 12th International Power Electronics and Motion Control Conference*. IEEE, 2006, pp. 1–17.
- [4] A. El-Shahat, *Electric Machines for Smart Grids Applications: Design, Simulation and Control*. BoD—Books on Demand, 2018.
- [5] R. Kumar and B. Singh, "BLDC motor-driven solar PV array-fed water pumping system employing zeta converter," *IEEE Transactions on Industry Applications*, vol. 52, no. 3, pp. 2315–2322, 2016.
- [6] S. Sashidhar and B. Fernandes, "A novel ferrite SMDS spoke-type BLDC motor for PV bore-well submersible water pumps," *IEEE Transactions on Industrial Electronics*, vol. 64, no. 1, pp. 104–114, 2016.
- [7] R. Kumar and B. Singh, "Grid interactive solar PV-based water pumping using BLDC motor drive," *IEEE Transactions on Industry Applications*, vol. 55, no. 5, pp. 5153–5165, 2019.
- [8] M. R. Feysi, S. K. M. Niapour, F. Nejabatkhah, S. Danyali, and A. Feizi, "Brushless DC motor drive based on multi-input DC boost converter supplemented by hybrid PV/FC/battery power system," in *2011 24th Canadian Conference on Electrical and Computer Engineering (CCECE)*. IEEE, 2011, pp. 000 442–000 446.
- [9] R. Kumar and B. Singh, "Single stage solar PV fed brushless DC motor driven water pump," *IEEE Journal of Emerging and Selected Topics in Power Electronics*, vol. 5, no. 3, pp. 1377–1385, 2017.
- [10] M. G. Villalva, J. R. Gazoli, and E. R. Filho, "Modeling and circuit-based simulation of photovoltaic arrays," in *2009 Brazilian Power Electronics Conference*, Sep. 2009, pp. 1244–1254.
- [11] O. Tremblay, L.-A. Dessaint, and A.-I. Dekkiche, "A generic battery model for the dynamic simulation of hybrid electric vehicles," in *2007 IEEE Vehicle Power and Propulsion Conference*. IEEE, 2007, pp. 284–289.
- [12] C. M. Shepherd, "Design of primary and secondary cells: Ii. an equation describing battery discharge," *Journal of the Electrochemical Society*, vol. 112, no. 7, p. 657, 1965.
- [13] P. Pillay and R. Krishnan, "Modeling, simulation, and analysis of permanent-magnet motor drives. ii. the brushless dc motor drive," *IEEE transactions on Industry applications*, vol. 25, no. 2, pp. 274–279, 1989.
- [14] A. Sangwongwanich, Y. Yang, and F. Blaabjerg, "High-performance constant power generation in grid-connected PV systems," *IEEE Transactions on Power Electronics*, vol. 31, no. 3, pp. 1822–1825, 2015.
- [15] V. Ramanarayanan, "Course material on switched mode power conversion," *Indian Institute of Science*, 2006.
- [16] R. W. Erickson and D. Maksimovic, *Fundamentals of power electronics*. Springer Science & Business Media, 2007.
- [17] R. Sheehan and L. Diana, "Switch-mode power converter compensation made easy," *Texas Instruments: Dallas, TX, USA*, 2016.